4. VERIFICATION OF THE MODEL

4.1 INTRODUCTION

In the previous chapter, the principles of fatigue crack propagation modeling were presented and an algorithm for 'model F' given. Before the 'model F' can be applied to analyze fatigue behavior, it must be compared with the fatigue test data, and limits of application established. The aim of this chapter is to investigate if the model developed can be applied to fatigue crack propagation simulations. The following two topics will be discussed :

– *quantitative comparisons* of simulated and measured fatigue-crack-propagation-related data ;
– *qualitative comparisons* of simulated and observed aspects of fatigue crack propagation.

The quantitative comparisons include the comparison of the simulated data to the fatigue crack propagation data of the *plate with a welded attachment* ; the comparison of the simulated data to the fatigue crack propagation data of the *plate with a center hole* ; the comparison of simulated *fatigue thresholds* to measured fatigue thresholds ; and the comparison of the simulated *crack closure* to the measured crack closure and to other crack closure models. The qualitative comparisons deal with the following aspects of fatigue crack propagation : *variable-amplitude load effects*, the *effect of nominal mean stress* and *small crack behavior*, *plate thickness effect*, and *fatigue behavior under cyclic compression*. The components of the quantitative and qualitative comparisons are shown in Figure 4.1.

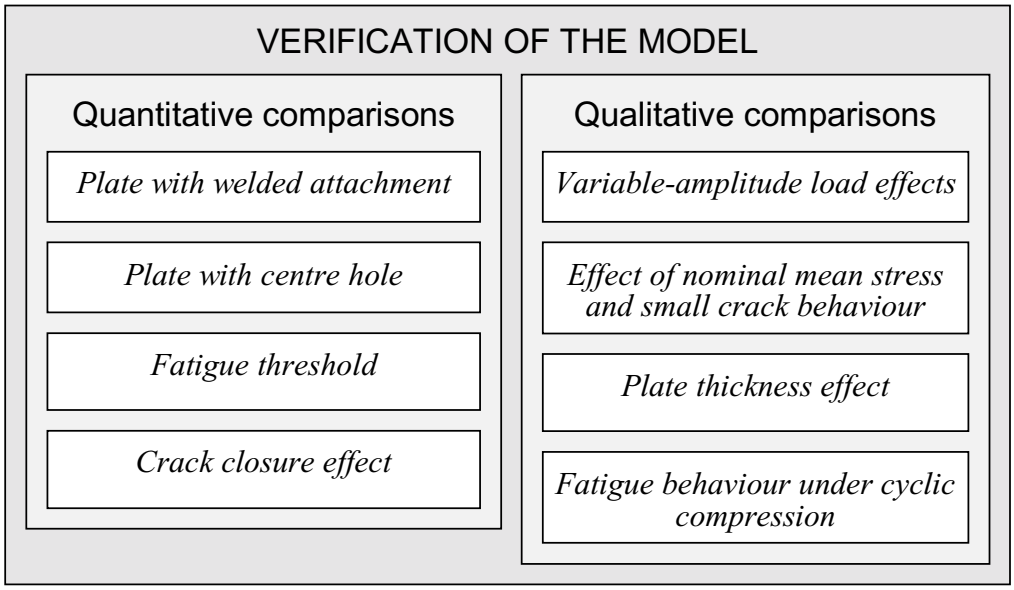

Figure 4.1 : *Parts of the verification.*

4.2 QUANTITATIVE COMPARISONS

4.2.1 Plate with Welded Attachment

The fatigue behavior of welded details is generally characterized by a relatively short crack initiation life when compared to the stable crack growth life. Therefore, this comparison

should reveal if the 'model F' is able to simulate the stable crack growth. The fatigue test data selected for this comparison is from Dubois [4.1].

Test Conditions

The *specimen geometry* is presented in Figure 4.2. The specimens tested by Dubois were fabricated in the workshop. Dubois [4.1] studied the influence of residual stresses on the fatigue behavior. The test specimens of Dubois were placed in three groups depending on the residual stress distribution along the crack path:

1. AW (as welded) specimens. It is assumed that there are mainly tensile residual stresses in the plate ;
2. HT (heat treated) specimens : heated for 4 hours, and then gradually cooled down in air 24 hours in order to reduce as much as possible, the residual stresses. It is assumed that this type of specimen is free of residual stress ;
3. NP (needle peening) specimens with weld toes treated using needle peening to improve their fatigue resistance. It is assumed that needle peening introduces compressive residual stresses in the upper layer of the plate at weld toe.

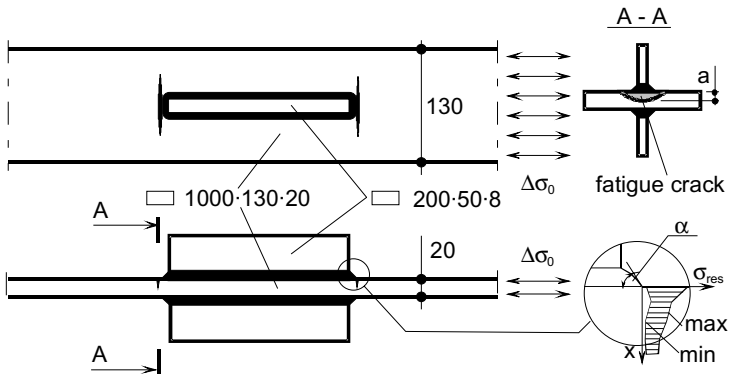

Figure 4.2 : *Tested specimen geometry, [4.1] (dimensions in [mm]).*

Three different *load histories* were applied to the specimens (Figure 4.3). The heat treated detail (HT) was only tested under constant-amplitude loading. The detail without treatment (AW), as well as the needle peened (NP) specimens, were tested for each of the three load cases.

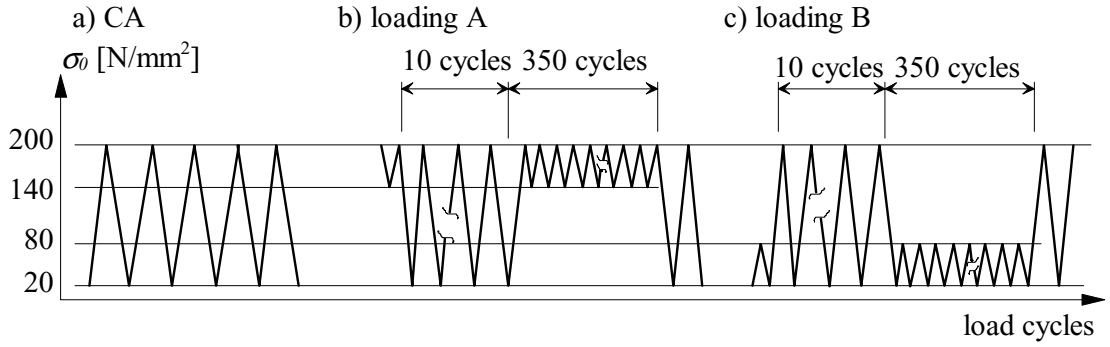

Figure 4.3 : *Load cases : a) constant-amplitude ; b) spectrum A ; c) spectrum B.*

The *material properties* of the test specimens required for the simulations were calculated *indirectly* : the chemical composition and the monotonic stress-strain data of the steel

Fe E 355 indicated in [4.1] were used in order to choose the steel that has best agreement with the properties from [4.2]. The test fitting was found for steel *St50*. Both initial and obtained material parameters are presented in Table 4.1.

Tests were conducted at room temperature and the crack propagation curves were measured using the potential drop method [4.3], [4.4].

Quantity, parameter	Tested material [4.1]	Most corresponding material [4.2]
Test temperature	20° C	20° C
Rough material	20 mm thick plate	20 mm thick plate
Chemical composition		
C [%]	0.17	0.15
Si [%]	0.35	0.35
Mn [%]	1.14	1.40
P [%]	0.017	0.015
S [%]	0.009	0.012
Ni [%]	0.013	0.01
Mechanical parameters		
σ'_{ys} [N/mm^2]	379	385
σ_f [N/mm^2]	543	534
A_5 [%]	28	31
E [N/mm^2]	210000	206000
σ'_{ys}		329
K'		957
n'		0.172
σ'_f		829
b'		-0.098
ε'_f		0.415
c'		-0.565

Table 4.1 : *Identification of material cyclic stress-strain and fatigue properties : steel St50.*

Numerical simulations of the fatigue crack propagation are made using the geometrical, loading and material parameters which correspond to the tested specimens. In order to obtain the variation of simulated crack propagation curves, the lower and the upper boundary of the measured residual stress bands, $\sigma_{res}=max$ and $\sigma_{res}=min$, are used. The second parameter varied is the weld toe angle, α. The values of α, used in the numerical simulation are : $\alpha = 40^o$ and $\alpha = 60^o$. The stress concentration factor *SCF*, and the stress intensity factor *K*, depend on the variation of the residual stress and the weld toe angle. The calculation of *SCF* and *K*, was made similarly to [4.1].

Comparison of Simulated and Measured Data

In the following discussion, 7 comparisons between the simulated and measured data are presented. Each comparison includes two types of curves : *a-N* curves and *da/dN-a* curves. The comparisons are grouped according to the loading used : the *constant-amplitude* data is given in Figure 4.4, the data according to *loading A* is shown in Figure 4.5, and the data due to *loading B* in Figure 4.6. The variation of the simulated curves is obtained by changing the weld toe angle α, and the distribution of the residual stress (see Figure 4.2). The residual stress distributions are taken from [4.1].

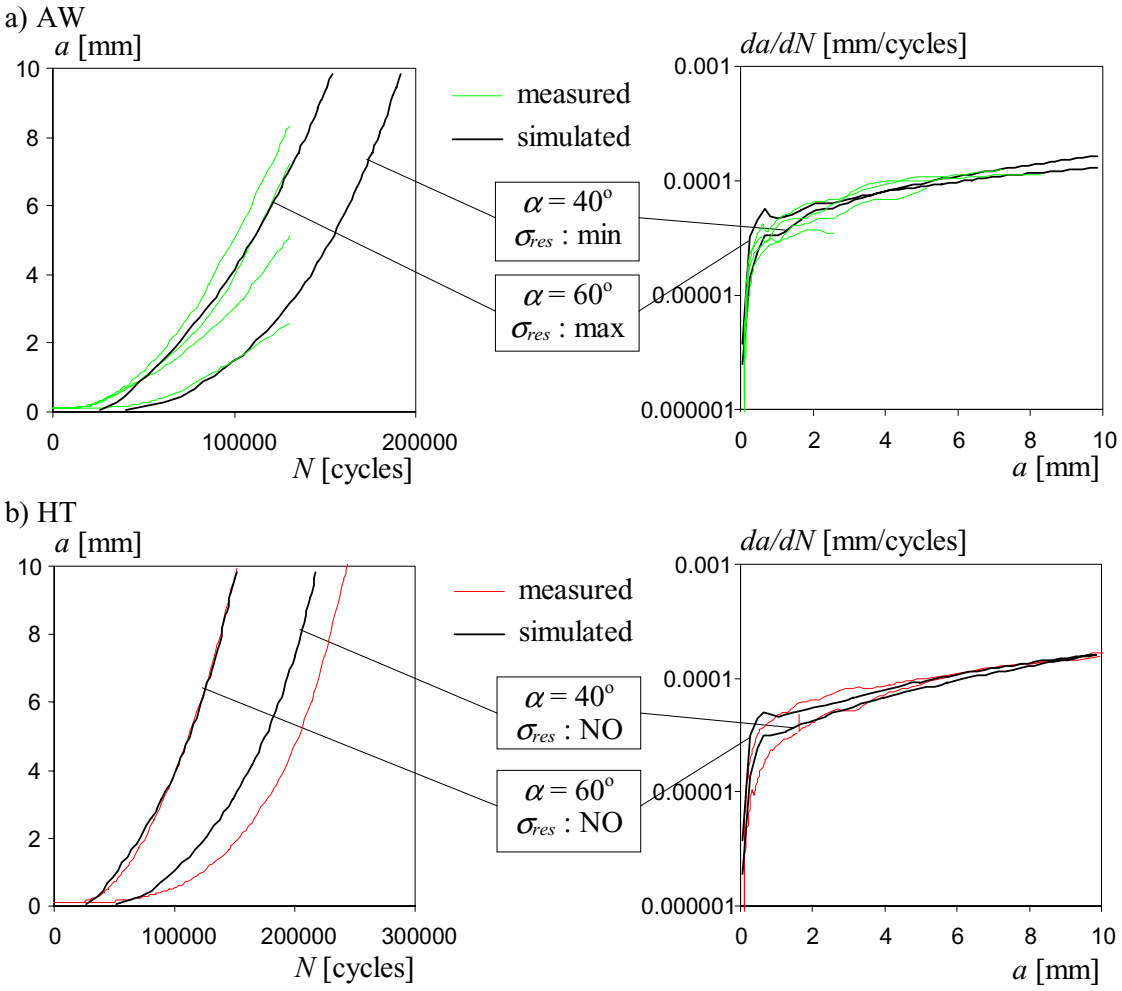

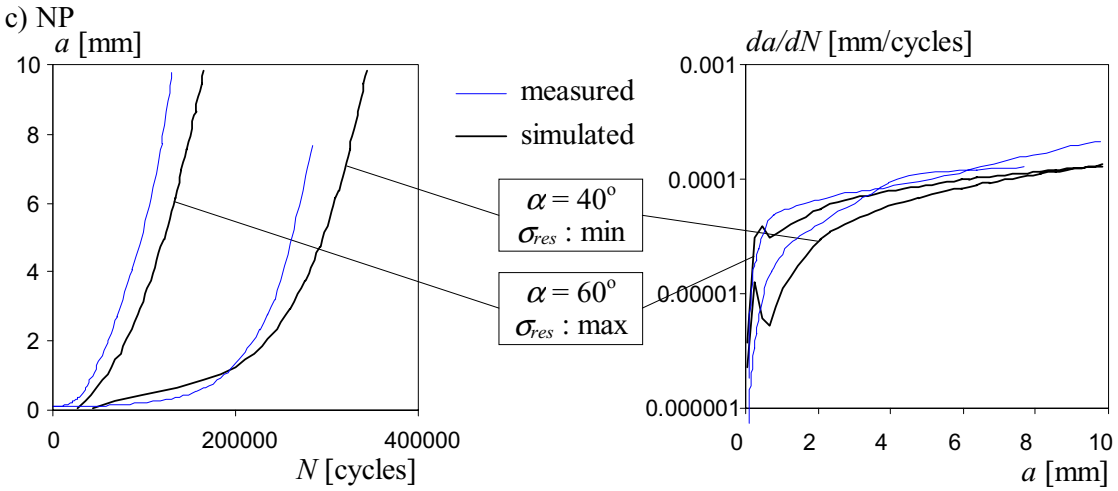

Figure 4.4 : *Comparison of simulation results to the test data [4.1] : constant-amplitude loading ; a) as welded specimen ; b) heat treated specimen ; c) needle peened specimen.*

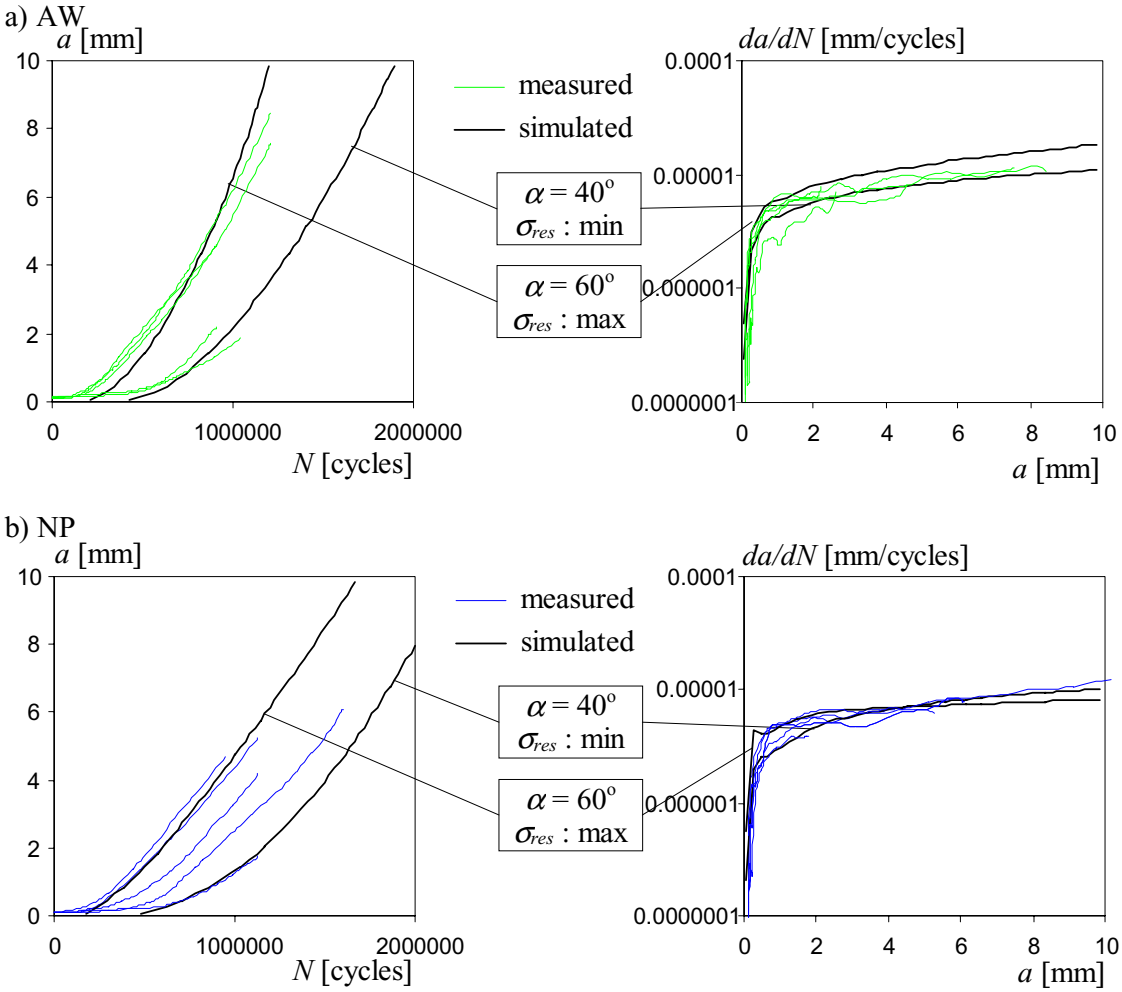

Figure 4.5 : *Comparison of simulation results to the test data [4.1] : loading A ; a) as welded specimen ; b) needle peened specimen.*

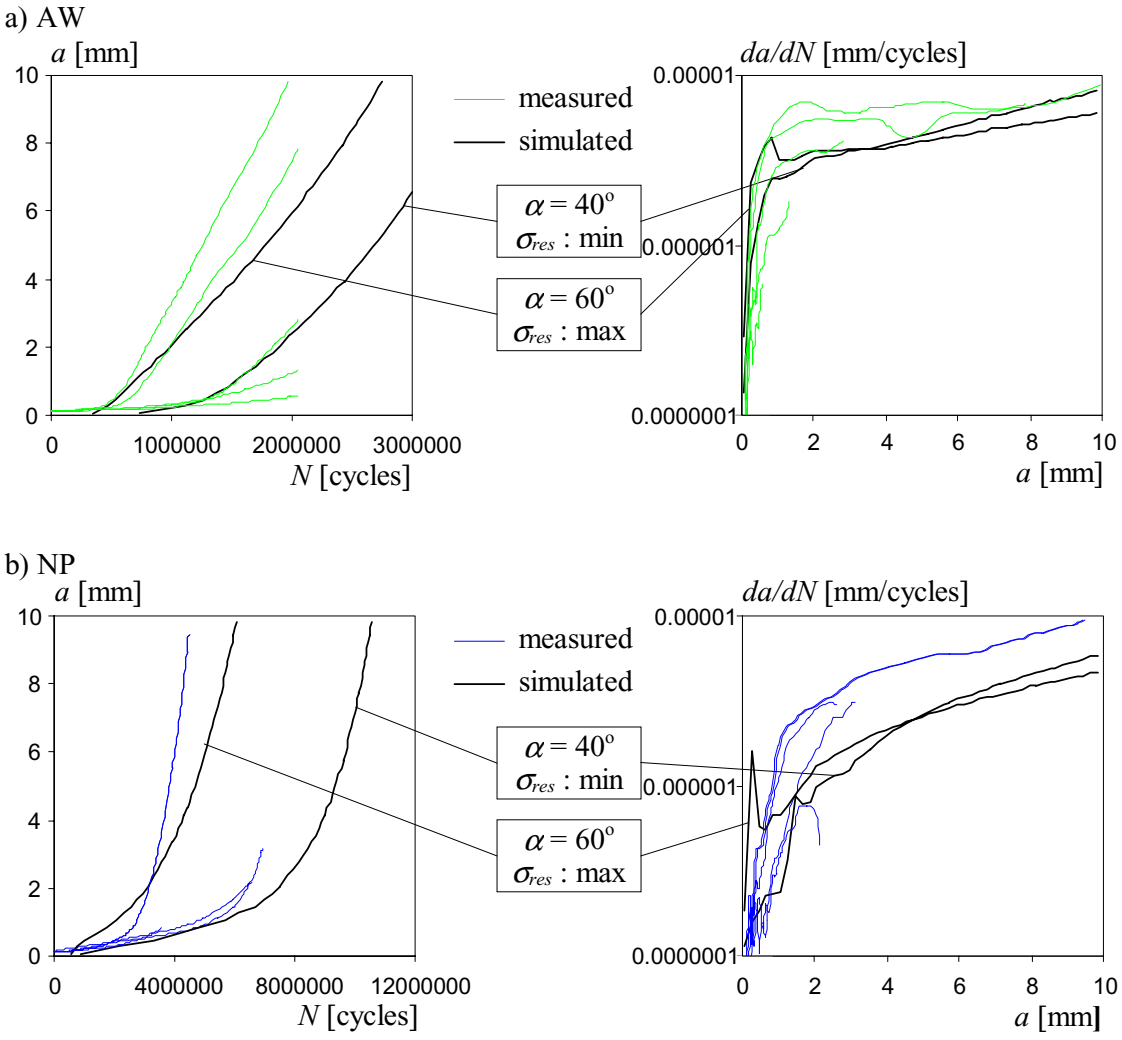

Figure 4.6 : *Comparison of simulation results to the test data [4.1] : loading B ; a) as welded specimen ; b) needle peened specimen.*

The comparison generally shows good and very good agreement between the simulated and measured data. The agreement is good for both types of curves compared: *a-N* curves and *da/dN-a* curves. Only in the case of *loading B*, the comparison is satisfactory and not good. One of the reason of satisfactory agreement can the uncertainties in the residual stress distribution used in simulations : the distribution of the residual stress, used in simulation is approximate, and does not correspond to the exact distribution of the residual stress in the details. It must be noted that the 'non-regularities' of simulated *da/dN-a* curves occur due to non-uniform distribution of the residual stress and due to small crack behavior.

Based on the results of the comparisons, it can be concluded that the 'model F' can be applied to the fatigue analysis of the details which show a *short* crack initiation life and a *long* stable crack growth life[1], and to the analysis of the influence of fabrication induced residual stresses. Comparisons show that there is a strong correlation between simulated and measured fatigue crack propagation curves.

[1] Although *no* crack initiation period was assumed by Dubois [4.1], it can be supposed that the crack initiation life exists, but it is very *short* : the horizontal parts of the measured *a-N* curves can be considered as indicators of the crack initiation stage.

4.2.2 Plate with Center Hole

The fatigue behavior of plates with a hole in the center is generally characterized by a relatively *long* crack initiation life compared to the stable crack growth life. The following comparison should show under which conditions, if any, the 'model F' is able to simulate the crack initiation. Fatigue tests referenced in this section were carried out at the Swiss Federal Laboratories for Materials Testing and Research (EMPA).

Test Conditions

The *Specimen geometry* is presented in Figure 4.7. The plates were fabricated in the workshop using a hot-rolling process. The residual stresses inside the plate generated during fabrication are not known and their influence on the fatigue behavior is not taken into account.

Quantity	Tested material	Corresponding material, [4.2]
Test temperature	23° C	23° C
Rough material	10 mm thick plate	sheet
Chemical composition		
C [%]	0.12	0.09
Si [%]	0.25	0.22
Mn [%]	0.97	1.07
P [%]	0.012	0.017
S [%]	0.021	0.008
Ni [%]	0.09	-
Mechanical parameters		
σ_{ys} [N/mm^2]	364	384
σ_f [N/mm^2]	495	457
A_5 [%]	29.7	27
E [N/mm^2]	197500	206000
σ'_{ys}		311
K'		1053
n'		0.196
σ_f'		733/755
b'		-0.083
ε_f'		0.198/0.204
c'		-0.440

Table 4.2 : *Identification of material cyclic stress-strain and fatigue properties : steel St 42.*

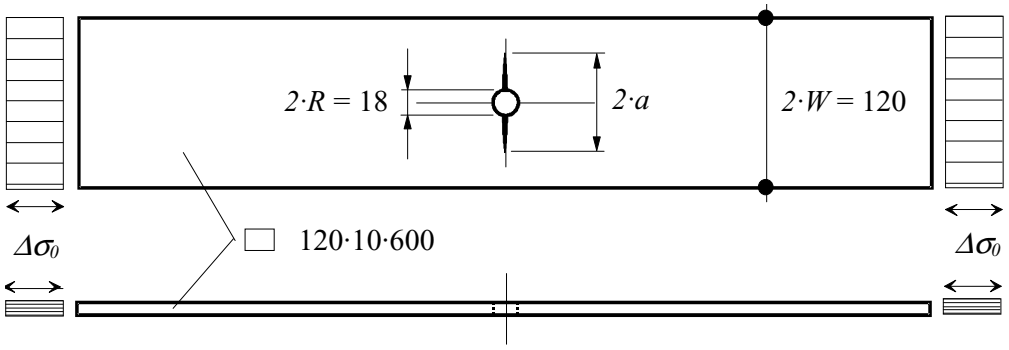

Figure 4.7 : *Tested specimen geometry (dimensions in [mm]).*

The material properties of the test specimens needed for the simulations were calculated *indirectly* : monotonic stress-strain data of the steel used, was obtained from monotonic tensile of material bars. Material bars were cut out from the plates so that their longitudinal axis corresponded to the longitudinal axis of the plate. The chemical composition of the steel was also determined. Monotonic stress-strain data were obtained and chemical composition was compared to the data in [4.2]. Then, the steel that had the best corresponding properties was chosen from [4.2]. It was found that the properties of the *St42* steel were the closest to the measured material properties. The initial and obtained material parameters are shown in Table 4.2.

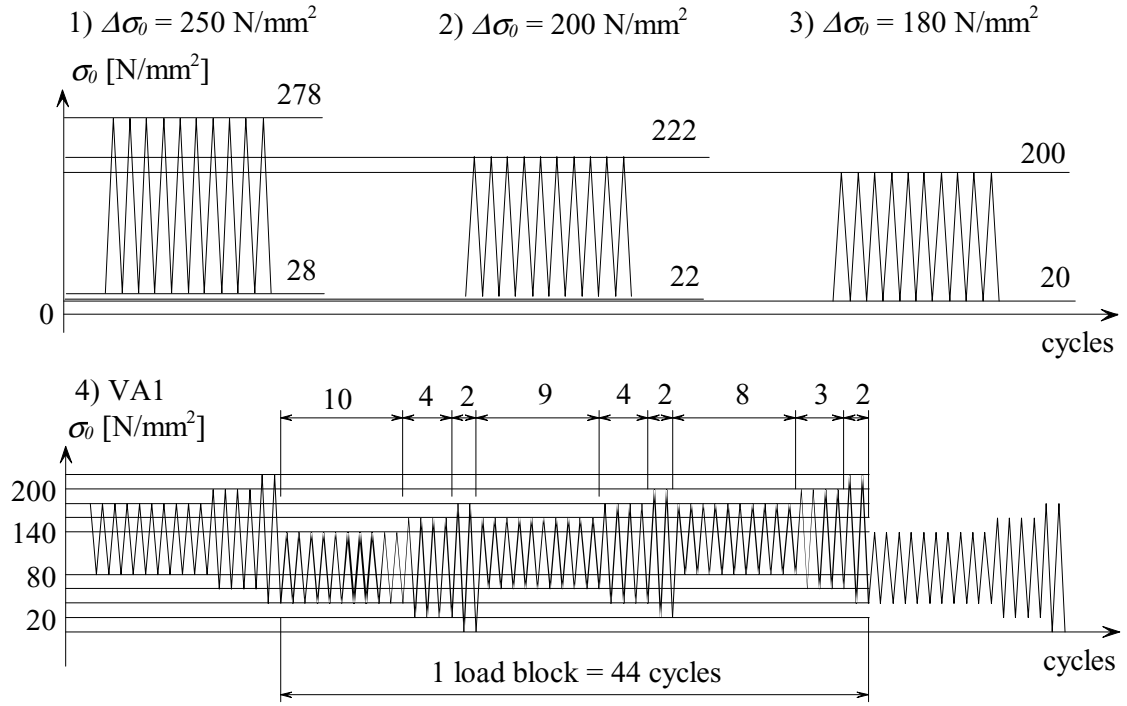

Figure 4.8 : *4 load cases, applied on test specimens.*

The *loading* cases used in the tests were :
1. constant-amplitude load, with $R = 0.1$, and $\Delta\sigma_0 = 250$ N/mm^2 ;
2. constant-amplitude load, with $R = 0.1$, and $\Delta\sigma_0 = 200$ N/mm^2 ;
3. constant-amplitude load, with $R = 0.1$, and $\Delta\sigma_0 = 180$ N/mm^2 ;

4. variable-amplitude load blocks[1] (VA1) ;
5. variable-amplitude load blocks (VA2 = VA1·1.1) ;
6. variable-amplitude load blocks (VA3 = VA1/1.2).

The four first loading cases are presented in Figure 4.8. The difference between the cases VA1 and VA2 is that in the load history VA2 all stress peaks are 1.1 times *greater* than the stress peaks in load history VA1. The difference between the cases VA1 and VA3 is that in the load history VA3, all stress peaks are 1.2 times *smaller* than the stress peaks in load history VA1.

Numerical simulations of the fatigue crack propagation are made using geometrical, loading and material parameters which correspond to the tested specimens. Distribution of the stress concentration factor *SCF(x)* was determined using an analytical solution given in [4.5]. The stress intensity factor *K* was calculated as indicated in [4.6].

In order to obtain the variation of the simulated crack propagation curves, two material parameters; 1) the fatigue strength coefficient σ'_f and 2) the fatigue ductility coefficient ε'_f, were varied within the range indicated in Table 4.2. The variation of σ'_f and ε'_f results in two strain life relationships, noted A and B in Figure 4.9. Curves A and B are very close to the mean $\Delta\varepsilon$-N_f curve of steel St42.

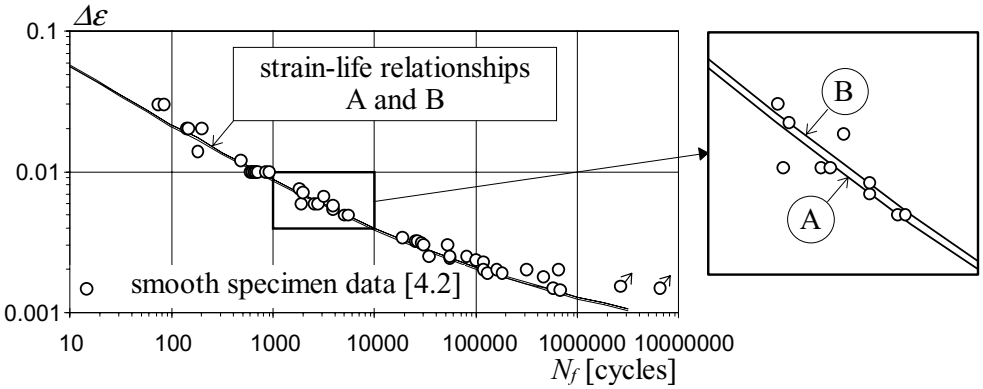

Figure 4.9 : *Strain-life relationships used in simulations.*

Comparison of Simulated and Test Results

Comparison of simulated results for the *constant-amplitude* fatigue test data is presented in Figure 4.10. The difference between compared crack propagation curves is less than 12%. It can be concluded that the used material data correspond to the tested steel.

Two tests were conducted under *variable-amplitude* loading VA1. Crack propagation was only measured during the second test. The first test however, yielded two data for the *a-N* graph : The point corresponding to the moment when the crack was not yet initiated, and the point corresponding to the final crack length.

One test was carried out under loading VA2. Results of variable-amplitude fatigue tests are presented in Figure 4.11. A comparison of simulated results to the fatigue test results indicates that there is a *bad* agreement between simulated and measured crack propagation data. Specifically, the shapes of simulated and measures curves correspond well, but test cracks *initiate* about 2.5...3 times faster than predicted by 'model F'.

No crack initiation occurred during the fatigue test under loading VA3, and the test was stopped after 10 million load cycles. The *simulation* using 'model F', however, predicted

[1] Choice of the variable-amplitude load spectrum is arbitrary.

crack initiation. Specifically, the strain life curve 'A' predicted N_{CI}=*7'039'400* cycles, and the strain life curve 'B' predicted: N_{CI}=*8'583'400* cycles.

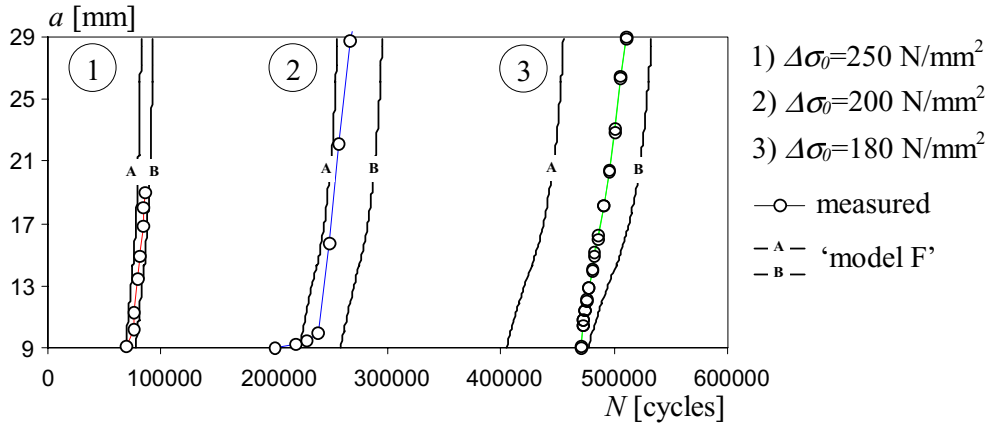

Figure 4.10 : *Comparison of simulation results to the constant-amplitude fatigue test data.*

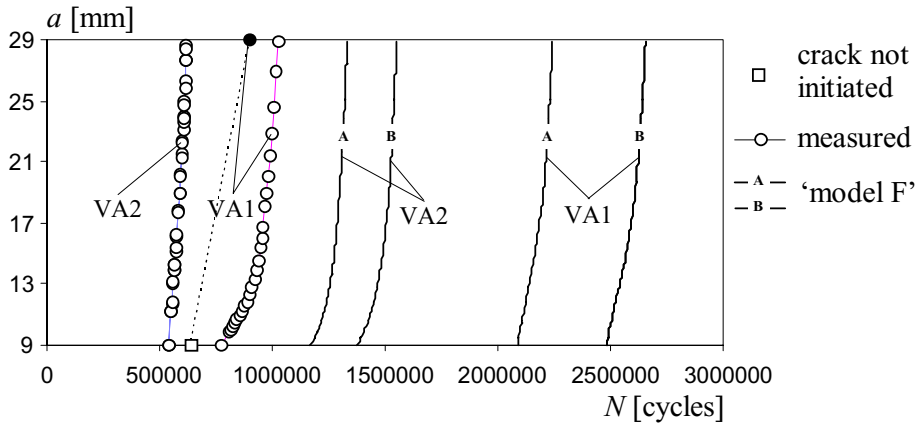

Figure 4.11 : *Comparison of simulation results to the data of the variable-amplitude fatigue tests VA1 and VA2.*

The bad agreement between measured and simulated data may be due to the larger scatter of material properties rather than the scatter of material properties of constant-amplitude fatigue tests. However, the large scatter of material properties does not entirely explain the bad agreement : it seems that 'model F' is non-conservative if the applied *variable-amplitude* loads are high, and conservative if the applied *variable-amplitude* loads are small. It was not possible to explain this bizarre disagreement between the simulation and variable-amplitude test results.

It can be concluded that under *constant-amplitude* loading, the 'model F' can successfully be applied for fatigue analysis of details which exhibit a *long* crack initiation life and a *short* stable crack growth life e.g., plates with center hole (see CA tests). On the other hand, under variable-amplitude loading, simulation results are conservative (see test VA3) if load ranges are small, and non-conservative if they are high (see tests VA1 and VA2).

4.2.3 Fatigue Threshold

The purpose of this section is to verify if the 'model F' is capable of simulating the fatigue threshold. The fatigue threshold is often evaluated using the threshold stress intensity factor range, ΔK_{th}. The ΔK_{th} is determined using the *da/dN-ΔK* curve which is obtained from the analysis of measured fatigue propagation curves. The threshold stress intensity factor range on the *da/dN-ΔK* curve corresponds to the crack propagation rate :

$$\left(\frac{da}{dN}\right)_{th} \cong 10^{-8} \text{ [mm/cycle]} \tag{4.1}$$

'Model F' is based on the strain-life relationship, which is used to calculate fatigue life of elements. The strain-life relationship does not account for the fatigue threshold and there are no special features included in the 'model F' to account for the fatigue threshold. It can be assumed, however, that in cases where the effective stress intensity factor range ΔK_{eff} leads to the average *simulated* crack propagation rate $(da/dN)_{th}$, a fatigue threshold is reached and $\Delta K_{eff}=\Delta K_{th}$.

Figure 4.12 represents the comparison between the modeled ΔK_{th} and the ΔK_{th}, as found in the literature : [4.1], [4.7], [4.8]. The comparison shows that the agreement between the measured and simulated fatigue threshold is *good*. In addition to the good agreement, there is another threshold-related argument on the favor of the 'model F' . It is well known that fatigue the threshold is influenced by the nominal mean stress [4.9], [4.10], [4.11]. The strain life relationship, used in the modeling, accounts for the effect of the nominal mean stress. Thus the 'model F' takes into account the influence of the mean stress on the fatigue threshold. It can be concluded that 'model F' is *able* to simulate the fatigue threshold.

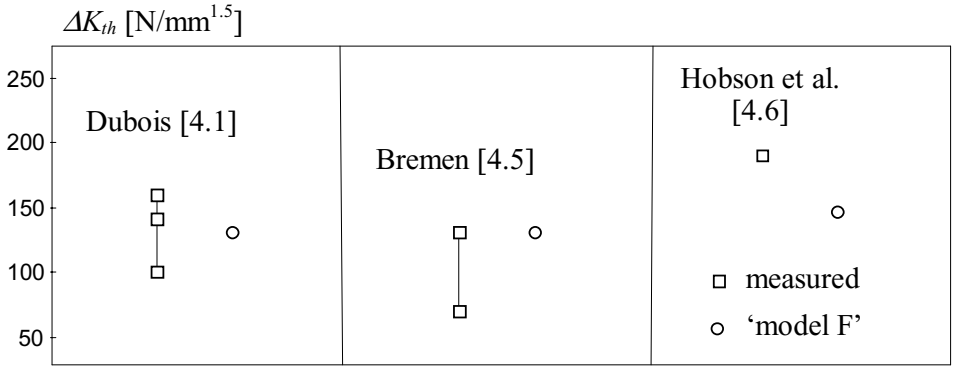

Figure 4.12 : *Comparison of the measured and simulated fatigue thresholds.*

4.2.4 Crack Closure Effect

The purpose of this section is to verify if the crack closure model, developed in section 3.5 and used in 'model F', is able to take into account the crack closure effect. The verification can be made by comparing the crack opening stresses, σ_{op}. The crack opening stresses depend mainly on the cyclic yield stress, σ'_{ys}, the minimum and maximum nominal stresses, $\sigma_{0,max}$ and $\sigma_{0,min}$, and the plastic constraint factor, *pcf*. The variables, σ_{op}, σ'_{ys}, $\sigma_{0,max}$, and $\sigma_{0,min}$ are all related. When making comparisons, it is better to use normalized quantities instead these four parameters. The normalization is given in Annex A.3, and it results in the following three parameters; 1) the effective stress ratio R_{eff}, 2) minimum and maximum stress ratio R, and 3) the maximum and cyclic yield stress ratio R_{ys}.

Three types of comparisons are made - the effective stress ratios (R_{eff}) calculated using the developed crack closure model, are compared to the effective stress ratios calculated using :
– *nonlinear finite element* modeling ;
– *strip yield* models ;
– *empirical* formula.

Within each comparison, the effective stress ratio of a *linear* crack (crack in linearly behaving material) $R_{eff,le}$ is also given. The $R_{eff,le}$ can be calculated using Equation (4.2) :

$$R_{eff,le} = Max(R;0) \tag{4.2}$$

Comparison versus Non-Linear FE Modeling

Newman [4.12] has calculated the R_{eff}-R curve using a non-linear finite element analysis. In Figure 4.13, the results obtained by Newman are compared to the simulated results. Newman has calculated the R_{eff}-R curve for two levels of the maximum and cyclic yield stress ratio : $R_{ys}=0.3$ and $R_{ys}=0.4$.

The comparison shows that the two R_{eff}-R curves, simulated using the 'model F', agree better with each other than the corresponding curves calculated using the non-linear finite element modeling. Within the region $0 \le R < 1$, however, the agreement between the 'model F' simulated and the finite-element-modeled R_{eff}, is *very good*.

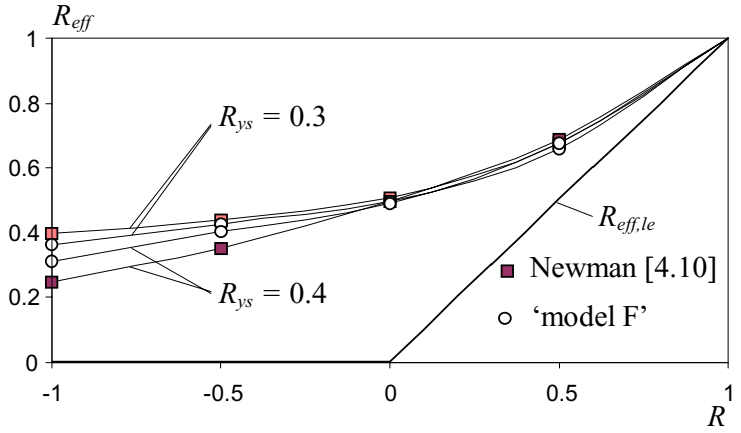

Figure 4.13 : *Comparison of simulated R_{eff}-R curves to R_{eff}-R curves, obtained using the FEM [4.12].*

Comparison versus Strip Yield Models

The crack closure effect is often modeled using the so-called strip yield models [4.13], [4.14]. The advantages of the strip yield models, when compared to finite element calculations, are that they do not require the generation of the finite element mesh. The required CPU time for the strip yield modeling is also much smaller than the required CPU time for nonlinear finite element modeling. The disadvantage of strip yield models is they result in less accuracy when compared to finite element modeling.

Wang and Blom [4.13] showed that a strip yield model can simulate the crack closure phenomenon for a wide range of details under arbitrary loading histories. Their model was probably the first which was capable of simulating *all* important crack closure related fatigue aspects. Figure 4.14 presents the comparison of the R_{eff}, simulated using two different models; 1) Wang's and Blom's strip yield model and 2) the crack closure model in 'model F'.

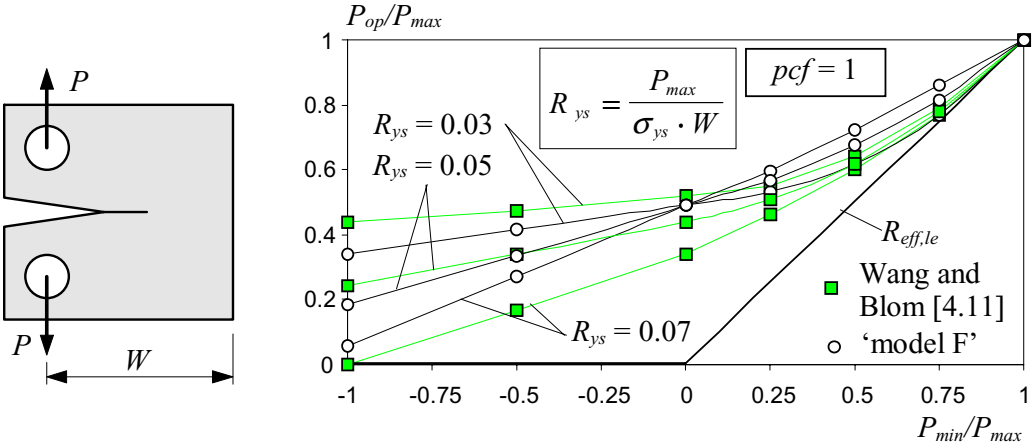

Figure 4.14 : *Comparison of the simulated R_{eff}-R curves to R_{eff}-R curves, obtained using the strip yield model [4.13].*

The comparison shows that the results do not agree well, especially if $R_{ys} = 0.07$. One of the reasons for the poor agreement is that within the closure model, developed in Section 3.5, the crack profile function of the *Dugdale* crack is used. The crack profile function of the Dugdale crack differs from the crack profile function of the CT-specimen. Thus the discrepancy of between the effective stress ratios R_{eff} is expected. On the other hand, it can be that for : $R \leq -1$ and $R_{ys} \geq 0.07$, the strip yield model of Wang and Blom does yield non-accurate predictions.

Another strip yield model was developed by Cheng and Yamada [4.14] and it is slightly different from the model in [4.13]. Cheng and Yamada modeled a finite width plate with a saw cut at the center. A crack initiates at the ends of the saw cut. A comparison of R_{eff} taken from [4.14] and R_{eff}, simulated with the 'model F', is presented in Figure 4.15. The results agree very well except at the region where $R \approx 0.8$. In this region, the R_{eff} values from [4.14], show strange behavior. It can be seen that the slope of the curve changes abruptly and joins the curve of the $R_{eff,le}$. It was not possible to find some rational explanation for this behavior.

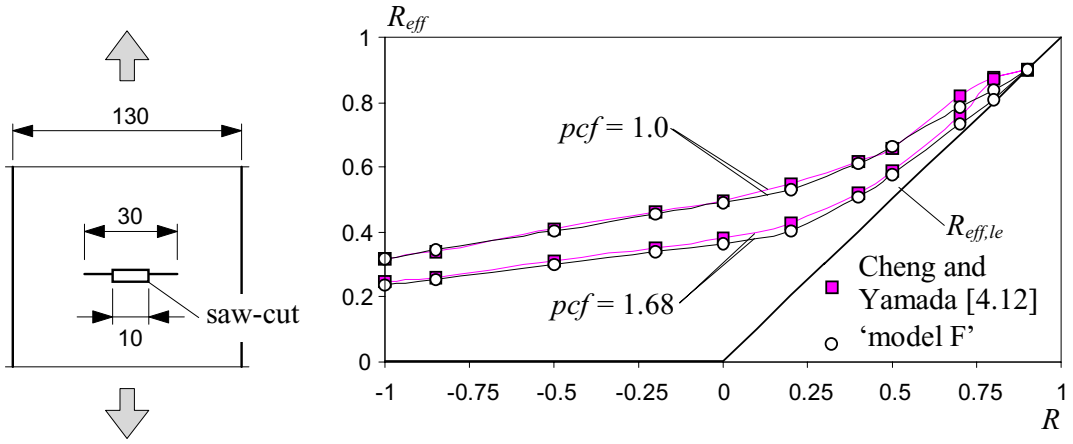

Figure 4.15 : *Comparison of simulated R_{eff}-R curves to the R_{eff}-R curves, obtained using the strip yield model [4.14].*

Comparison versus Empirical Formula

Veers [4.15] proposed an empirical formula to calculate the R_{eff} that is based on the analysis of the measured opening stress:

$$R_{eff} = Max\left[q_0 \cdot \left(1 + \frac{R}{R_0} \right); R \right] \tag{4.3}$$

Material parameters q_0 and R_0 are determined from testing and vary within the range determined by Equations (4.4) and (4.5). Equations (4.4) and (4.5) can be considered as the limits of application for Equation (4.3) because they determine the upper and the lower bound of the equation.

$$q_0 \in [0.2...0.5] \tag{4.4}$$

$$R_0 \in [-5...-2] \tag{4.5}$$

The upper and the lower bound of the Equation (4.3) can be fitted using the 'model F' if the plastic constraint factor (*pcf*) and the maximum and cyclic yield stress ratio R_{ys} vary within the range determined by Equations (4.6) and (4.7). A Comparison of the effective stress ratios calculated using the 'model F' and equations (4.3), (4.4) and (4.5) is presented in Figure 4.16. It can be seen that there is good agreement between compared curves.

$$pcf \in [1... 3] \tag{4.6}$$

$$R_{ys} \in [0.2...0.8] \tag{4.7}$$

Conditions (4.6) and (4.7) determine the limits of application for the crack closure model developed: condition (4.6) indicates that the crack closure model can be applied to all possible plate thicknesses. Combining conditions (4.7) and (A.10) leads to the limits for the $\sigma_{0,max}$:

$$0.2 \cdot \sigma'_{ys} \le \sigma_{0,max} \le 0.8 \cdot \sigma'_{ys} \tag{4.8}$$

It can be concluded that the crack closure model, developed within this study and utilized in 'model F', can be applied for the calculation of crack opening stresses within the limits determined by conditions (4.6) and (4.8).

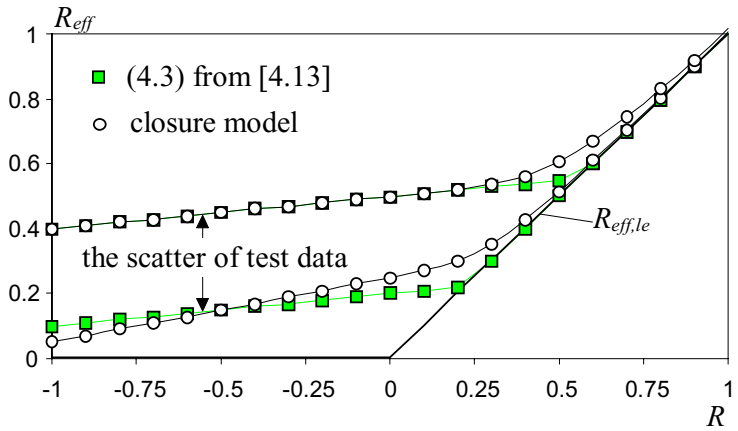

Figure 4.16 : *Comparison of the simulated R_{eff}-R curves to Equation (4.3).*

4.3 QUALITATIVE COMPARISONS

The aim of this section is to establish if the 'model F' is able to simulate special aspects of fatigue crack propagation, as discussed in Clause 2.3.3. The verifications are carried out in form of *qualitative* comparisons. In other word, the *shapes* of simulated and measured crack propagation curves are compared. These Comparisons consider *four* specific aspects of fatigue crack propagation: 1) variable-amplitude load effects, 2) small crack behavior and effect of nominal mean stress, 3) specimen thickness effect, and 4) crack behavior under cyclic compression.

4.3.1 Variable-amplitude Load Effects

The 'model F' includes a *crack closure model* that simulates the effects of variable-amplitude loading on fatigue crack propagation. In this section, the ability of the crack closure model to simulate the variable-amplitude load effects will be shown. Four common variable-amplitude loading cases are considered : tensile overload, compressive overload, tensile overloads followed by compressive overload, and change in nominal mean stress. In the following, the effect of these loading cases on the simulated fatigue crack propagation is reviewed.

Tensile Overload

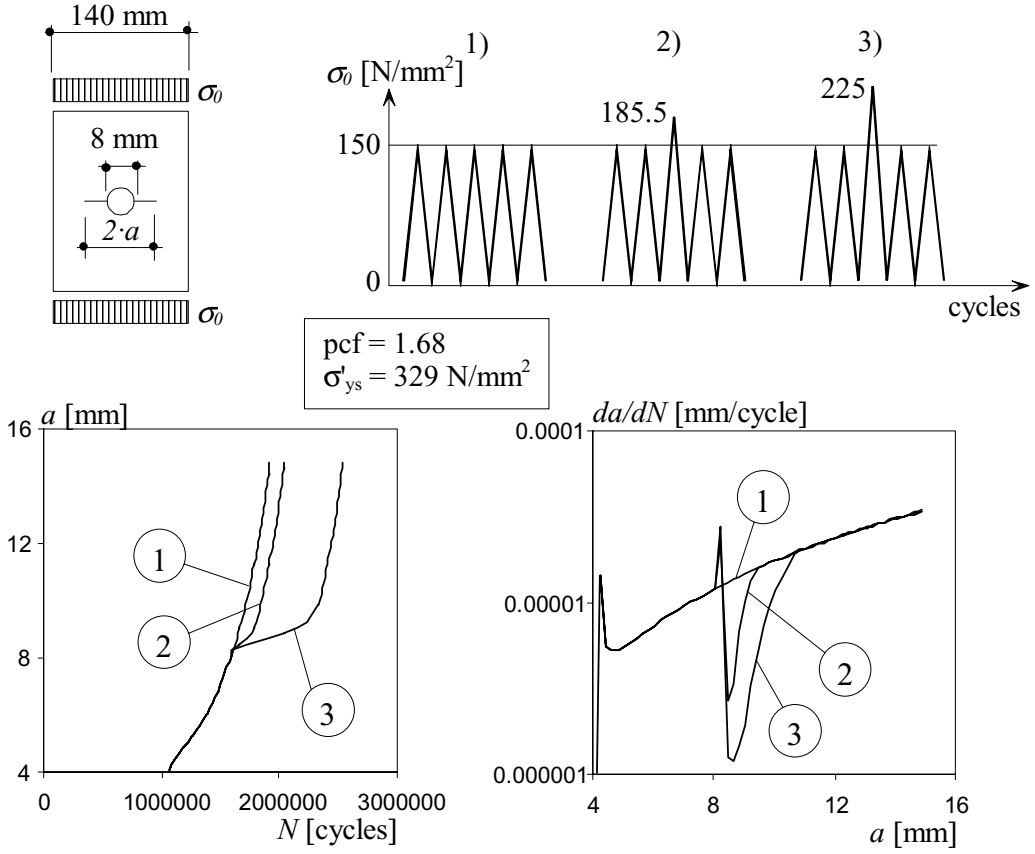

Figure 4.17 : *Retardation effect due to tensile overload.*

In Figure 4.17 the simulation results at three loading cases of tensile overload are shown. The ratio of the overload to the nominal maximum stress was selected as : $\sigma_{0,TOL}/\sigma_{0,max}$=*1, 1.25* and *1.5*. Both simulation results *and* published data indicate that :
- crack propagation accelerates and then rapidly slows down just after application of the overload. This leads to a sharp peak in the *da/dN-a* curve [4.16].
- Delay of the retardation depends on the magnitude of the overload [4.13].
- Retardation of the crack propagation due to the overload does not only depend on the magnitude of the overload, but also on the moment in time when the overload was applied. The plate thickness[1] and the ratio of the maximum nominal stress to the yield stress R_{ys} [4.10], [4.16] also effect crack propagation.

The qualitative comparison shows a *good* agreement between simulations and published data on the effect of tensile overload.

Compressive Overload

Compressive overloads have no effect on the *simulated* crack propagation. This is in agreement with the results from the literature: [4.14], [4.17]. However, the effect of a compressive overload depends on the specimen *geometry* and the magnitude of the compressive overload. (CT-specimens, for example, show an acceleration of the crack propagation if compressive overload(s) are applied [4.18]).

Tensile Overload Followed by Compressive Overload

Three loading cases were simulated in order to show the effect of tensile overload followed by compressive overload. The ratios of compressive and tensile overload $\sigma_{0,COL}/\sigma_{0,TOL}$, were taken to be 0, 0.33 and 0.67, respectively. The ratio of the maximum nominal stress and the tensile overload was kept constant : $\sigma_{0,TOL}/\sigma_{0,max}$ = *1.5*. Simulated crack propagation curves are given in Figure 4.18.

Both the simulation results *and* published data show that :
- the retardation effect of the tensile overload is significantly reduced if followed by the compressive overload [4. 14], [4.16].
- Acceleration of the crack propagation just after application of the tensile and compressive overloads is more significant than in the case of the tensile overload [4.14].
- Shortening of the retardation period depends on the magnitude of the compressive overload [4.14].

The qualitative comparison shows a *good* agreement between simulations and published data about the effect of tensile overload followed by compressive overload.

[1] Thickness effect in the 'model F' is taken into account through the plastic constraint factor *pcf*.

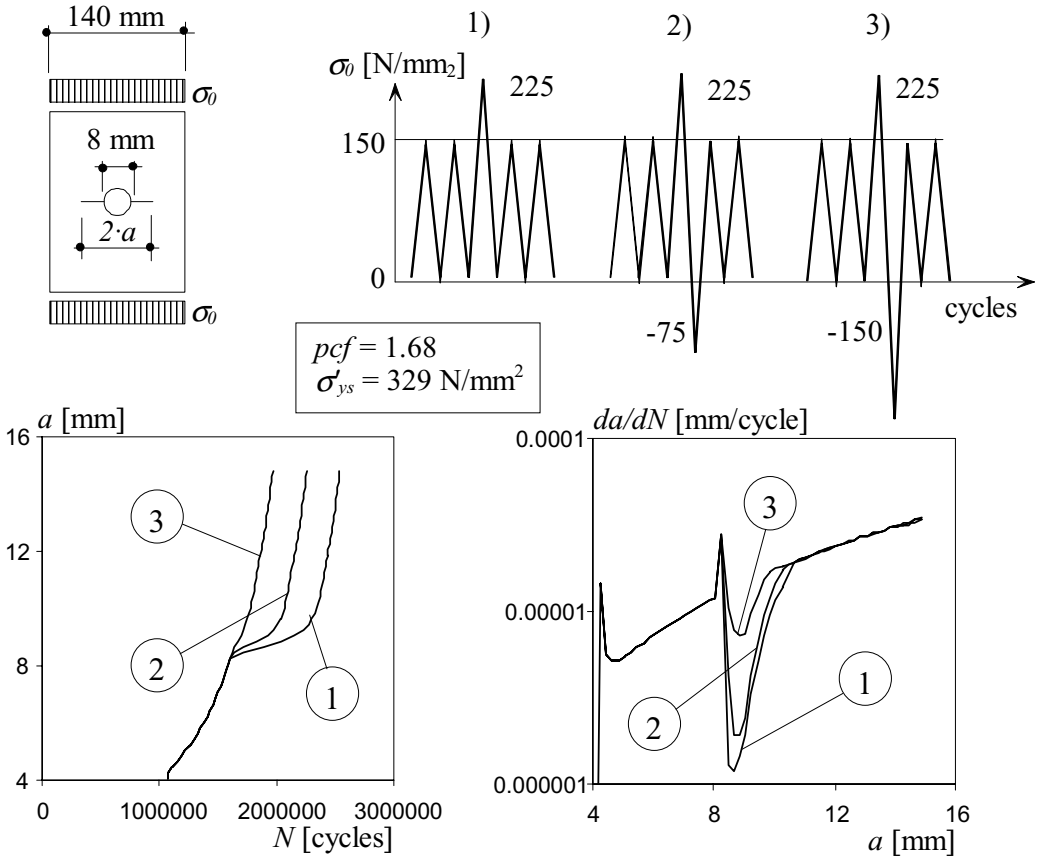

Figure 4.18 : *Influence of a tensile overload followed by the compressive overload.*

Change in Nominal Mean Stress

Three loading cases were simulated in order to show the effect of change in nominal mean stress on the crack propagation. These three cases were as follows; 1) the mean stress was kept *unchanged*; 2) the mean stress was *increased* by a factor 1.33 during the crack propagation; 3) the mean stress was *decreased* by factor 1.33. The *simulated* crack propagation curves are given in Figure 4.19. Both simulation results *and* published data show that :

- a sudden increase in the mean stress causes an acceleration of the crack propagation rate *da/dN* (the sharp peak in Figure 4.19, case 2). As time increases, the crack velocity will decrease, however if will remain above the curve of the preliminary mean stress [4.13].
- A sudden decrease in the mean stress causes a retardation of the crack propagation rate *da/dN* (the sharp trough in Figure 4.19, case 3). As time increases, the crack velocity will increase but will remain below the curve of the preliminary mean stress [4.13].

The qualitative comparison shows *good* agreement between simulations and published data on the effect of the change in nominal mean stress.

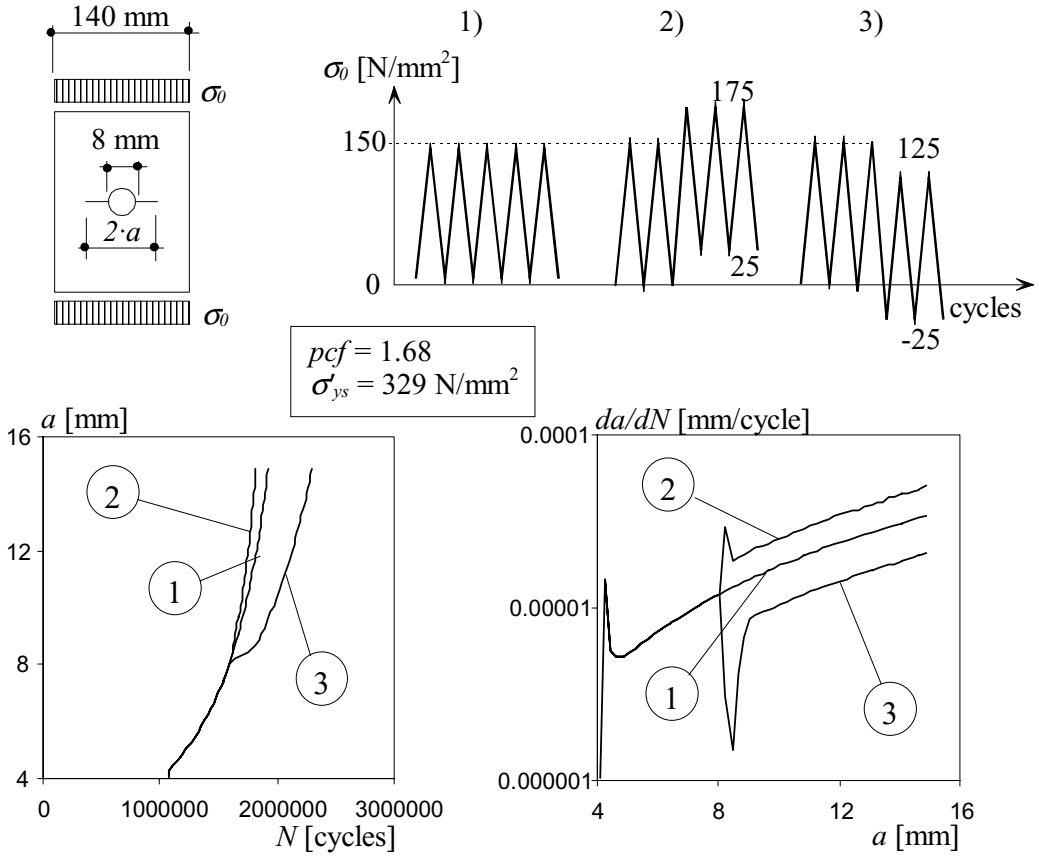

Figure 4.19 : *The effect of nominal mean stress on the fatigue behavior.*

4.3.2 Effect of Nominal Mean Stress and Small Crack Behavior

Effect of Nominal Mean Stress

There are two features included in the 'model F' which allow simulation of the effect of *nominal mean stress* ; 1) use of the strain-life relationship, and 2) use of the crack closure model. Three loading cases are simulated in order to show the effect of the nominal mean stress on the crack propagation. The three nominal mean stress simulated are 150, 100 and 50 N/mm^2. The nominal stress range is kept constant at $\Delta\sigma_0$=200 N/mm^2. *Simulated* crack propagation curves are given in Figure 4.20. Both simulated results *and* published data show that a high nominal mean stress leads to faster crack initiation [4.19] *and* faster stable crack growth [4.19], [4.10]. It is concluded that there exists a *good* agreement between simulated results and published data regarding the effect of nominal mean stress on the crack propagation.

Small Crack Behavior

There are two features included in the 'model F' which allow simulation of *small crack behavior*: 1) the consideration of the simultaneous damaging of elements, and 2) the use of the crack closure model. The results of simulated small crack behavior can be seen in Figure 4.20. (Note the regions of the small crack behavior are indicated on the *a-N* curves and on the *da/dN-ΔK* curves). The simulated phenomenon agrees well with the phenomenon observed during actual fatigue tests [4.20]. It can be concluded that the 'model F' can simulate such complex fatigue phenomenon as small crack behavior.

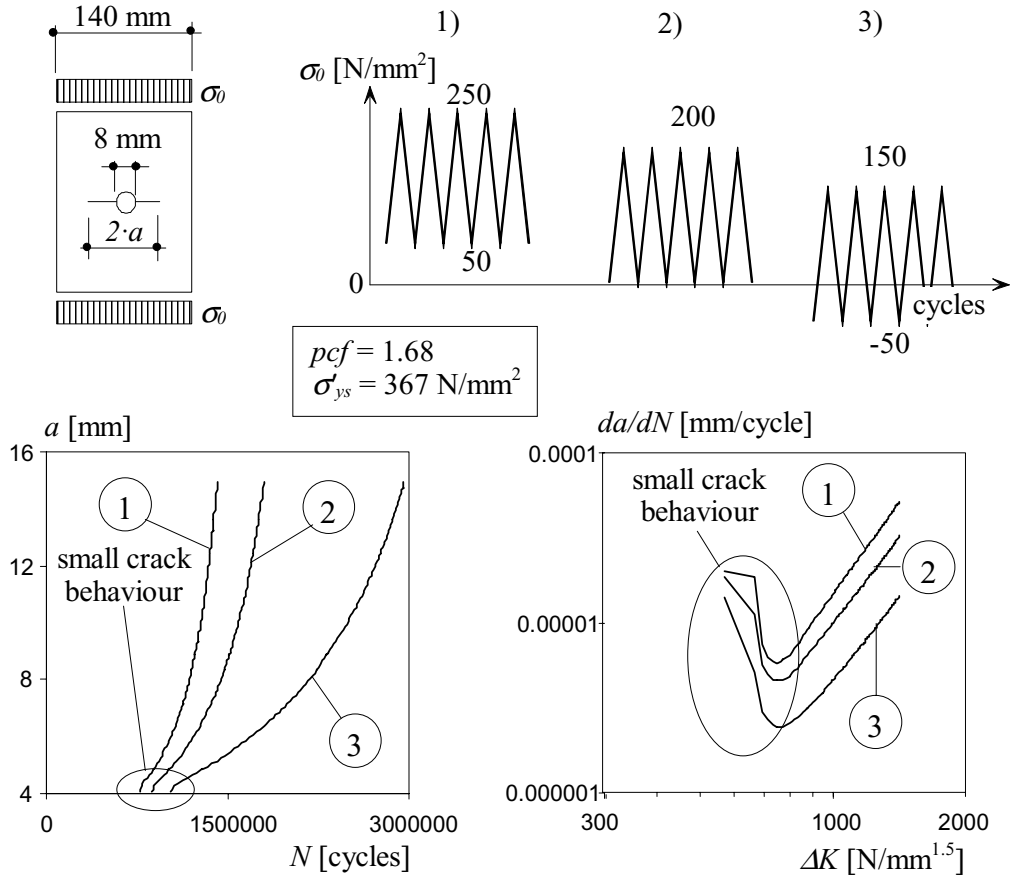

Figure 4.20 : *Simulated small crack behavior.*

4.3.3 Specimen Thickness Effect

The specimen thickness effect is considered in the 'model F' through the plastic constraint factor (*pcf*) included in the crack closure model. A *pcf=1* means that plain stress conditions prevail at the crack tip. This corresponds to a crack in a thin plate. If *pcf=3,* then plain strain conditions prevail at the crack tip. This corresponds to a crack in very thick plate. Three values of the plastic constraint factor were used in simulations: *pcf=1*, *2* and *3*.

Simulation results are presented in Figure 4.21 and show a *good* agreement with published data. The crack in a thin plate propagates much slower than a crack in a medium or in a thick plate [4.10], [4.21], [4.22]. Figure 4.21 also shows that the duration of the crack initiation stage is not influenced by the plate thickness effect. If the crack initiation takes place on the plate surface where a plane stress condition always prevails, then *pcf=1*.

An additional argument available to demonstrate that a fatigue crack propagates faster under plain strain conditions than under plain stress conditions follows. For a through crack in a thick plate (Figure 4.22), it is known that the crack length is always greater in the center of the plate than on plate surface ($a_{plane\ strain} > a_{plane\ stress}$). Condition $a_{plane\ strain} > a_{plane\ stress}$ indicates that the propagation is faster inside the plate where plane strain prevails and slower on plate surface, where plane stress prevails.

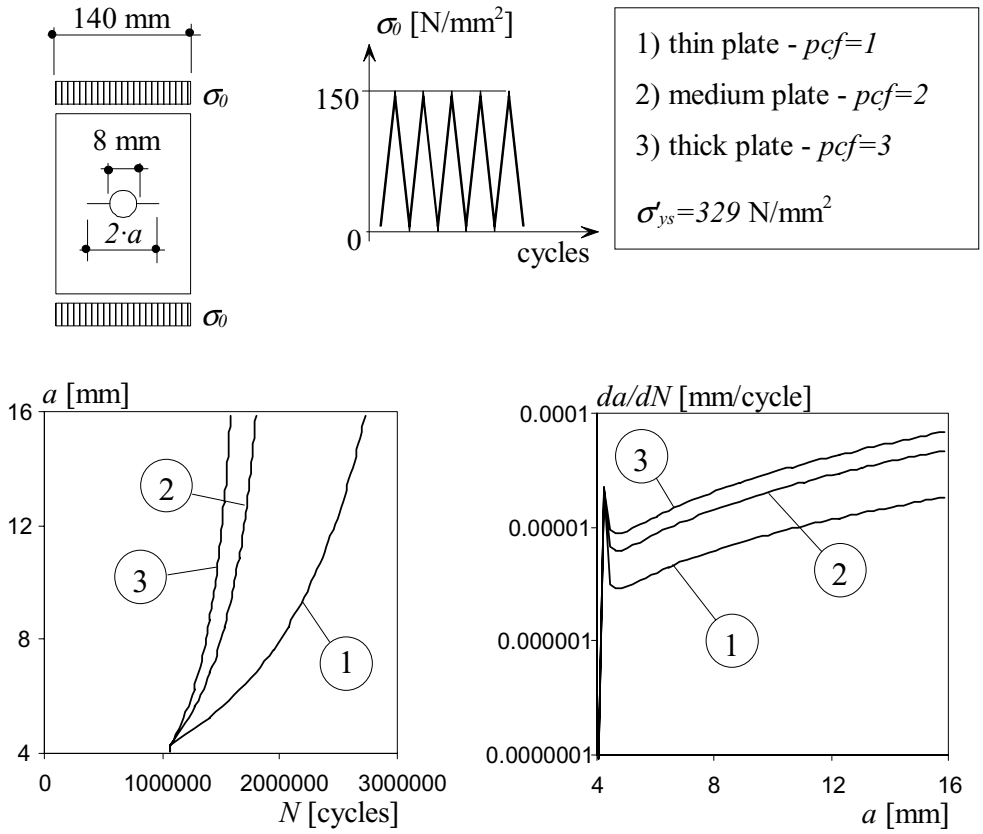

Figure 4.21 : *The effect of the variation of the plastic constraint factor on the fatigue behavior.*

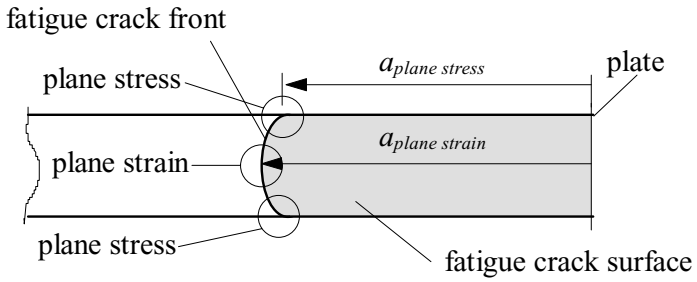

Figure 4.22 : *Fatigue crack lengths as a function of the plain strain and plain stress conditions.*

4.3.4 Crack Behavior under Cyclic Compression

If the detail is loaded by cyclic compressive forces, then *crack initiation* takes place, however, *crack growth* will arrest if the crack tip has propagated far enough away from the crack initiator. In this section the ability of the 'model F' to simulate the crack behavior under cyclic compression will be shown.

Simulations are carried out under three nominal mean stress ratios : $\sigma_{0,m}$=*-50*, *-100* and *-150* N/mm^2. The nominal stress range is kept constant: $\Delta\sigma_0$=*200* N/mm^2. The results of the simulation are presented in Figure 4.23. The simulations show that the crack initiation takes place during a relatively short time, but then slows down and finally stops (Figure 4.23). The

fatigue test data of cyclically compressed specimens [4.23], [4.24], demonstrate a behavior similar to what is shown in Figure 4.23. The first case in Figure 4.23 indicates that if the maximum nominal stress $\sigma_{0,max}$, is large enough, then the crack will not stop, however propagation will be very slow.

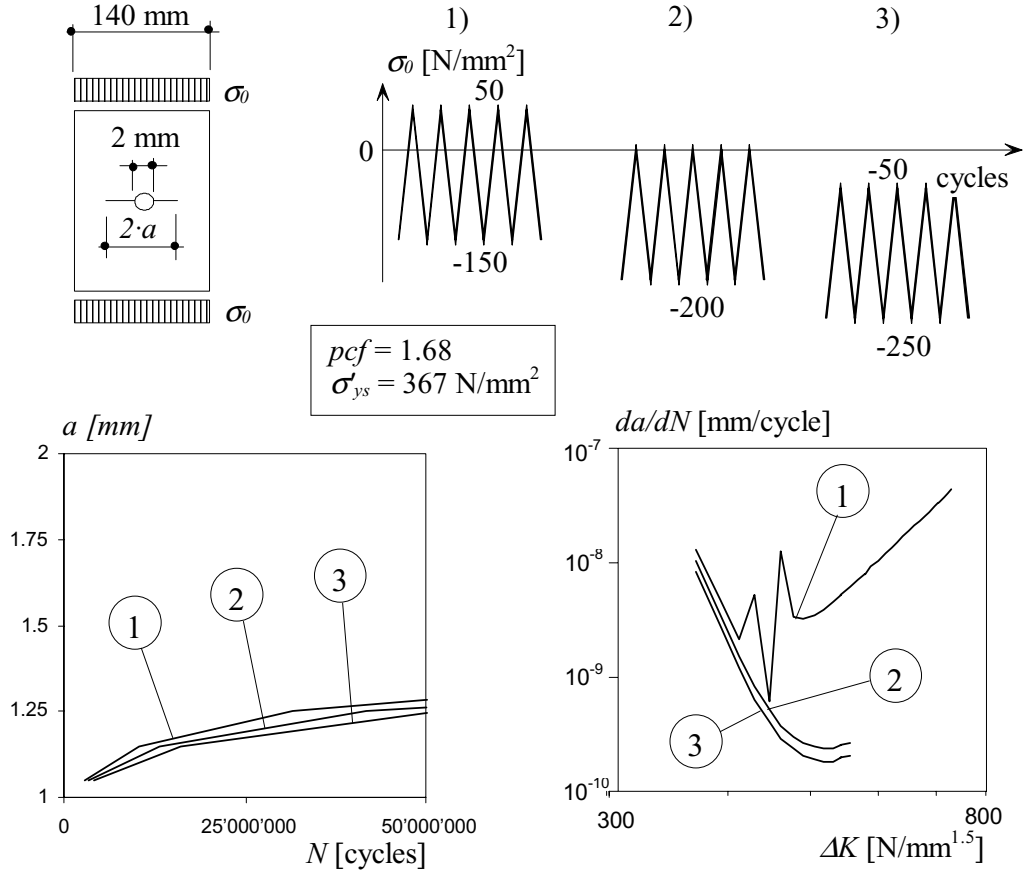

Figure 4.23 : *Crack initiation and stopping due to cyclic compression, simulated by 'model F'.*

4.4 SUMMARY AND CONCLUSIONS

The purpose of chapter 4 was to verify if the 'model F', developed in chapter 3, is applicable to fatigue analysis. Verification was carried out in form of quantitative and qualitative comparisons.

Quantitative Comparisons

A quantitative comparison means a collation of simulated and measured fatigue data. Such a quantitative comparison was applied on four types of data; 1) on the crack propagation curves of the plate with welded attachment, 2) on the crack propagation curves of the plate with center hole, 3) fatigue threshold stress intensity factors, and 4) R_{eff}-R curves. Comparisons generally showed a good agreement between simulated and measured data, except for the case of a plate with center hole loaded by the variable-amplitude loading. In this case, the agreement between simulated and measured crack initiation period was not satisfactory.

Qualitative Comparisons

A qualitative comparison means a collation of *shapes* of compared curves. Qualitative comparisons were used to verify the ability of the 'model F' to simulate selected aspects of the crack propagation. These four aspects were; 1)variable-amplitude load effects and the effect of nominal mean stress on fatigue crack propagation, 2) a small crack behavior, 3) the effect of specimen thickness, and 4) the crack behavior under cyclic compression. All simulated aspects of fatigue crack propagation agreed well with the data published in literature.